Enhanced weathering strategies for stabilizing climate and averting ocean acidification

Lyla L. Taylor[1], Joe Quirk[1], Rachel M. S. Thorley[1], Pushker A. Kharecha[2,3], James Hansen[2], Andy Ridgwell[4,5], Mark R. Lomas[6], Steve A. Banwart[7] and David J. Beerling[1]*

Chemical breakdown of rocks, weathering, is an important but very slow part of the carbon cycle that ultimately leads to CO_2 being locked up in carbonates on the ocean floor. Artificial acceleration of this carbon sink via distribution of pulverized silicate rocks across terrestrial landscapes may help offset anthropogenic CO_2 emissions[1-5]. We show that idealized enhanced weathering scenarios over less than a third of tropical land could cause significant drawdown of atmospheric CO_2 and ameliorate ocean acidification by 2100. Global carbon cycle modelling[6-8] driven by ensemble Representative Concentration Pathway (RCP) projections of twenty-first-century climate change (RCP8.5, business-as-usual; RCP4.5, medium-level mitigation)[9,10] indicates that enhanced weathering could lower atmospheric CO_2 by 30–300 ppm by 2100, depending mainly on silicate rock application rate (1 kg or 5 kg m^{-2} yr^{-1}) and composition. At the higher application rate, end-of-century ocean acidification is reversed under RCP4.5 and reduced by about two-thirds under RCP8.5. Additionally, surface ocean aragonite saturation state, a key control on coral calcification rates, is maintained above 3.5 throughout the low latitudes, thereby helping maintain the viability of tropical coral reef ecosystems[11-14]. However, we highlight major issues of cost, social acceptability, and potential unanticipated consequences that will limit utilization and emphasize the need for urgent efforts to phase down fossil fuel emissions[15].

Since 1992, over 190 nations agreed to limit anthropogenic CO_2 emissions to avoid 'dangerous' human-made climate change[16], yet massive expansion of fossil fuel extractions, including shale gas and tar sands, is allowing emissions to grow[17]. Avoiding dangerous climate change may therefore require the controversial deployment of carbon dioxide removal (CDR) schemes[4,18], so-called 'negative emissions' strategies whereby CO_2 is captured and removed from the atmosphere. The Fifth Assessment Report of the Intergovernmental Panel on Climate Change[12] and the US National Research Council Report[18] both recognized enhanced terrestrial weathering of silicate rocks as an important but poorly constrained CDR approach. At present, natural weathering of silicate and carbonate rocks consumes ~0.25 PgC yr^{-1} of atmospheric CO_2, which is ~3% of fossil fuel emissions[19] (~9–10 PgC yr^{-1}). Artificially accelerating this land-based CO_2 sink involves the intentional application of pulverized silicate rocks to vegetated landscapes to markedly enhance CO_2 consumption[1-5]. However, assessments so far have excluded primary drivers of soil mineral weathering, especially

terrestrial ecosystem processes and feedbacks from CO_2 and future climate change, limiting our understanding of its capacity to offset fossil fuel CO_2 emissions[12].

Here we present spatially resolved analyses of enhanced weathering by terrestrial ecosystems as a macro-engineering CDR option based on idealized cases for distributing pulverized silicate rocks in the tropics using multi-model ensemble projections (Coupled Model Intercomparison Project, CMIP5) of twenty-first-century climate change[9,10]. Our modelling framework includes climate–plant–soil linkages important for regulating mineral weathering by coupling a detailed weathering model with a dynamic global vegetation model and accounting for land surface hydrology, topography and lithology[6,7] (Methods). We assess effects of enhanced weathering on net CO_2 consumption and examine feedbacks on atmospheric CO_2 and ocean chemistry over the next century using a suite of five CMIP5 general circulation model (GCM) simulations (1° latitude × 1° longitude)[9,10] for each of two Representative Concentration Pathway scenarios (RCPs): RCP8.5 (business-as-usual), and RCP4.5 (medium-level stabilization of emissions); postscripts (8.5 and 4.5) denote radiative forcing (W m^{-2}) in year 2100 relative to year 1750 (Supplementary Information). Assessments are undertaken for various application rates of the igneous rocks dunite (>90% olivine, Mg$_2$SiO$_4$; ref. 3) and harzburgite (50–90% olivine), which are both commercially mined, and basalt, for which major resources exist in terrestrial large igneous provinces (LIPs; ref. 20) (Fig. 1). These rates fall within the range adopted in the early 1930s for rejuvenating European forest soils with basalt to encourage tree growth[21].

Our simulations indicate that terrestrial weathering can be markedly increased by distributing pulverized silicate rocks throughout the tropics (30° N to 30° S), potentially consuming hundreds of petagrams (1 × 10^{15} g) of CO_2 by 2100 (Fig. 1). Ensemble median CO_2 consumption by terrestrial weathering increases towards a maximum as the total rock applied increases, with olivine-rich dunite and harzburgite being about twice as effective as basalt for equivalent application rates (Fig. 1a–c). We present CO_2 consumption curves assuming mixing depths of 10 cm and 30 cm for each application rate; 10 cm is probably the minimum mixing depth, given intense precipitation events, the distribution of macropores, and bioturbation by invertebrates in tropical soils down to depths of 30–50 cm (Supplementary Information). In the model, CO_2 consumption by weathering increases when added rock grains mix deeper in the soil, particularly at the 5 kg m^{-2} yr^{-1}

[1]Department of Animal and Plant Sciences, University of Sheffield, Sheffield S10 2TN, UK. [2]Earth Institute, Columbia University, 475 Riverside Drive, New York 10027, USA. [3]Goddard Institute for Space Studies, NASA, 2880 Broadway, New York 10025, USA. [4]Department of Geographical Sciences, University of Bristol, Bristol BS8 1SS, UK. [5]Department of Earth Sciences, University of California, Riverside, California 92521, USA. [6]Department of Mathematics, University of Sheffield, Sheffield S10 2TN, UK. [7]Kroto Research Institute, North Campus, University of Sheffield, Sheffield S3 7HQ, UK. *e-mail: d.j.beerling@sheffield.ac.uk
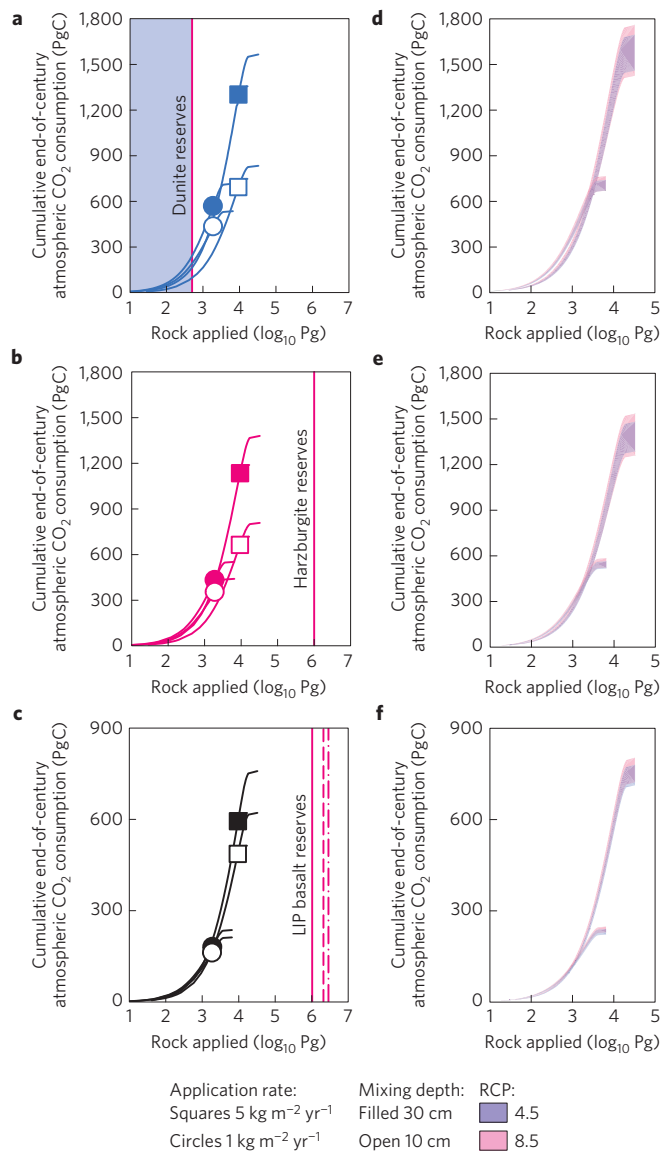
Figure 1 | Enhanced weathering from pulverized silicate rock additions to the tropics increases CO₂ consumption. a–c, End-of-century CO₂ consumption by enhanced terrestrial weathering with dunite (**a**), harzburgite (**b**), or basalt (**c**) as a function of total rock applied, defined as the product of rate and an increasing treated land area in the tropics (30° S to 30° N). Simulations are shown for the Representative Concentration Pathway (RCP) 8.5; median and range for five climate model simulations for each application scenario. Symbols indicate reductions in CO₂ consumption and total rock applied when application is limited to 20 Mkm² of tropical weathering hotspots; symbol shape and fill denotes application rate and mixing depth scenario, respectively, for each curve. Vertical red lines show estimated total resources for each rock type (for basalt, solid, dashed and dot-dashed lines represent basalt resources in the Ethiopian, Deccan and Paraná Traps, respectively). The shaded area denotes uncertainty in upper values of global dunite resource availability (Supplementary Information). **d–f**, Corresponding ensemble ranges using dunite (**d**), harzburgite (**e**), or basalt (**f**) for high and low application scenarios for each of five climate model simulations for both RCP8.5 and RCP4.5, assuming a mixing depth of 30 cm.
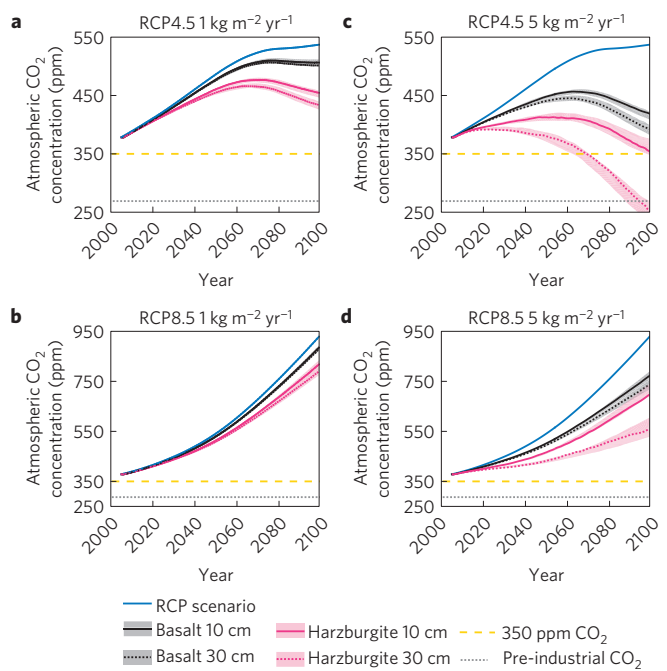
Figure 2 | Enhanced weathering lowers atmospheric CO₂ with projected twenty-first-century climate change. a,b, Effects of low additions of silicate rock to 20 Mkm² of tropical weathering hotspots for two mixing depths (10 cm and 30 cm) on the atmospheric CO₂ concentration for RCP4.5 (medium-level mitigation) (**a**) and RCP8.5 (business-as-usual) (**b**). **c,d**, As for **a,b**, but with higher additions of silicate rocks to the same areas of the tropics. In all panels, the pale blue line indicates the 'control' run with RCP-driven weathering, without additions of silicate rock. Envelopes and lines show the smoothed (five-year boxcar) ranges and medians, respectively, of results from five climate models for each RCP.

ensemble GCMs (Fig. 1d–f). For a given application rate, the magnitude of CO₂ consumption is similar for the business-as-usual (RCP8.5) and medium-level mitigation (RCP4.5) scenarios (Fig. 1d–f), largely because the runoff for the two scenarios is similar (Supplementary Information).

Comparing cumulative end-of-century amounts of pulverized rock added to the tropics with estimated total resources indicates dunite has limited utility for long-term atmospheric CO₂ removal[3] (Fig. 1), whereas sufficient harzburgite and basalt resources exist for the application rates considered here (Fig. 1, Supplementary Information). The rock mass required can be reduced by restricting application to regional intense tropical weathering 'hotspots' (Fig. 1 and Supplementary Information). Such optimization reduces the land area required by more than two-thirds, from 69 to 20 Mkm², and total rock mass by 70%, whilst still achieving ~80–89% of the effect (Fig. 1a–c, symbols). Hotspot land areas are primarily tropical forests, except parts of Asia which are croplands. However, basalt can promote crop growth on highly weathered acidic tropical soils[22,23] by increasing soil alkalinity, cation exchange capacity and the availability of growth-limiting phosphorus, with associated reductions in Al and Mn toxicity[23,24]. Ample basalt resources exist within the major LIPs in the tropics (Ethiopian Traps, Deccan Traps and Paraná Traps) to support simulated application rates (Fig. 1) and these sources could exploit existing infrastructure for distribution. Meeting silicate rock demand would require large-scale mining operations, for example, throughout the major tropical LIPs, with production rates exceeding those for coal and adverse consequences for local ecosystems.

As CO₂ is removed from the atmosphere by enhancement of the weathering carbon sink, the carbon cycle responds by

application rate, because mineral saturation, a chemical brake on weathering, occurs more slowly in a larger soil solution volume. Overall CO₂ consumption patterns for a particular RCP scenario show a consistently narrow range of variation across the five

Table 1 | Projected mean global air temperature and change in temperature at year 2100.

	Warming at 2100 (°C)		Warming averted at 2100 (°C)*	
	RCP4.5	RCP8.5	RCP4.5	RCP8.5
Control (no enhanced weathering)[†]	1.4 ± 0.01	3.0 ± 0.01	n/a	n/a
IPCC range of projected warming[‡] (ref. 12)	1.1–2.6	2.6–4.8	n/a	n/a
Enhanced weathering scenario				
Harzburgite ($1\,kg\,m^{-2}\,yr^{-1}$)	0.8 ± 0.04	2.5 ± 0.04	0.7 ± 0.04	0.5 ± 0.04
Harzburgite ($5\,kg\,m^{-2}\,yr^{-1}$)	-0.7 ± 0.2	1.4 ± 0.1	2.2 ± 0.2	1.6 ± 0.1
Basalt ($1\,kg\,m^{-2}\,yr^{-1}$)	1.2 ± 0.02	2.8 ± 0.01	0.2 ± 0.02	0.2 ± 0.01
Basalt ($5\,kg\,m^{-2}\,yr^{-1}$)	0.5 ± 0.05	2.3 ± 0.05	0.9 ± 0.05	0.7 ± 0.05

Values show mean ± s.d. of five climate models (CMIP5) for the change in end-of-century mean global temperature simulated with the GENIE Earth system model using revised CO_2 trajectories associated with each rock type and application rate with an applied rock mixing depth of 30 cm (Fig. 2). *Relative to control (no enhanced weathering); [†]Relative to 2005; [‡]Relative to 1986–2005.

redistributing carbon among surface reservoirs (atmosphere, ocean, soil, and land biosphere), with CO_2 out-gassing by the ocean in particular offsetting some of the artificial drawdown[17]. There is, consequently, a 'rebound' effect whereby each extra mole of CO_2 consumed does not translate into the removal of a mole of atmospheric CO_2 over time. We therefore estimate the effects of our CO_2 consumption fluxes on the RCP4.5 and RCP8.5 atmospheric CO_2 trajectories through the twenty-first century with the well-tested GENIE Earth system model[8], which broadly captures these responses. Distributing $1\,kg\,m^{-2}\,yr^{-1}$ of pulverized silicates across $20\,Mkm^2$ of tropical weathering 'hotspots' lowers atmospheric CO_2 concentrations by ∼40 ppm (basalt) or ∼140 ppm (harzburgite) by year 2100 in both the RCP4.5 and RCP8.5 climate change scenarios (Fig. 2a,b). Increasing the application rate to $5\,kg\,m^{-2}\,yr^{-1}$ over the same $20\,Mkm^2$ 'hotspot' areas lowers the atmospheric CO_2 concentration further by 150–180 ppm under both RCPs (Fig. 2c,d), with an increasing effect at deeper soil mixing depths. For RCP4.5, atmospheric CO_2 by 2100 is reduced from 540 ppm to 390–350 ppm (basalt) or 350–250 ppm (harzburgite), sufficient to play a major role in stabilizing climate and avoid seeding long-term amplifying climate feedbacks[17] (Fig. 2). For the business-as-usual RCP8.5 scenario, however, the lowest simulated CO_2 concentration by year 2100 in the high-end weathering scenario is still ∼730 ppm (basalt) or 690–560 ppm (harzburgite; Fig. 2d). This suggests even massive intervention in Earth's carbon cycle with basalt is unable to drive atmospheric CO_2 down close to the target of 350 ppm by 2100, an estimated requirement for restoring planetary energy balance and stabilizing climate[17].

Future climate warming averted by engineering CO_2 removal through enhanced weathering is dependent on climate sensitivity and the actual atmospheric CO_2 concentration. Calculated end-of-century 'warming averted' figures for the enhanced weathering scenarios using GENIE, which has a low-to-medium climate sensitivity, are summarized in Table 1. For high application rates, warming averted ranges from 0.9 to 2.2 °C for RCP4.5 and from 0.7 to 1.6 °C for RCP8.5 (Table 1). At low application rates, corresponding ranges of warming averted are 0.2–0.7 °C for both RCPs (Table 1). These numbers suggest that, theoretically at least, negative emissions from enhanced weathering could play a role alongside conventional mitigation reducing net CO_2 emissions in limiting future warming[25].

Unmitigated future increases in atmospheric CO_2 will not only drive climate change but also ocean acidification, including reduced saturation of surface waters with respect to aragonite, threatening reef-building coral ecosystems[11–14]. Artificially enhanced tropical weathering increases land-to-ocean fluxes of alkalinity and dissolved inorganic carbon, and raises freshwater pH to the upper range of tropical rivers (Supplementary Information). These fluxes, together with reduced atmospheric CO_2 (Fig. 2), tend to counter the negative impacts on ocean carbonate chemistry (Figs 3 and 4). Our simulations driven by decreased CO_2 (Fig. 2) and increased
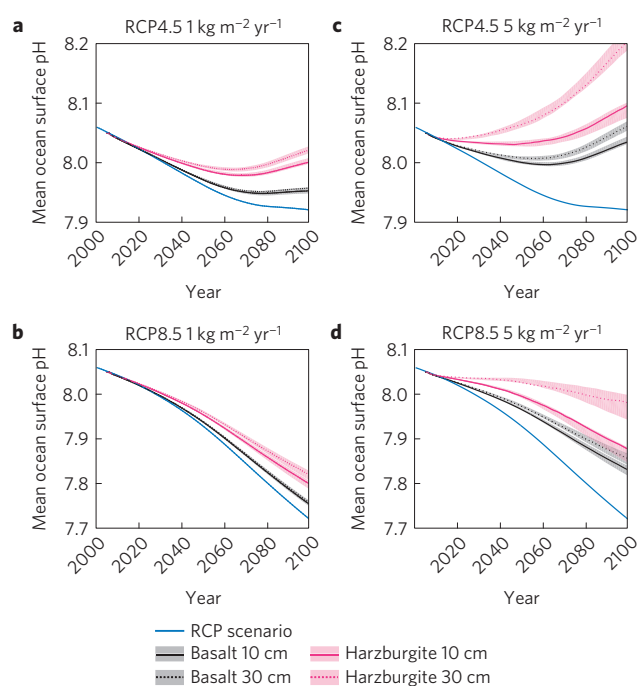
Figure 3 | Enhanced weathering ameliorates future ocean acidification caused by projected twenty-first-century increases in atmospheric CO_2. **a,b,** Effects of increased alkalinity fluxes resulting from additions of $1\,kg\,m^{-2}\,yr^{-1}$ of silicate rock to $20\,Mkm^2$ of tropical weathering hotspots mixed to two soil depths on global surface ocean pH for RCP4.5 (medium-level mitigation) (**a**) and RCP8.5 (business-as-usual) (**b**). **c,d,** Effects of increased alkalinity fluxes resulting from higher additions of silicate rocks to the tropics on global surface ocean pH for RCP4.5 (**c**) and RCP8.5 (**d**). Envelopes and lines show the smoothed (five-year boxcar) ranges and medians, respectively, of results from five climate models for each RCP.

alkalinity fluxes show that additions of $1\,kg\,m^{-2}\,yr^{-1}$ of harzburgite or basalt across the weathering 'hotspots' can mitigate future ocean acidification by an average of around 0.1 pH units (Fig. 3a,b). A higher silicate application rate ($5\,kg\,m^{-2}\,yr^{-1}$) reverses future surface ocean acidification under RCP4.5, restoring global mean surface ocean pH to year 2000 levels or even pre-industrial levels by 2100 (Fig. 3c). Even for RCP8.5, $5\,kg\,m^{-2}\,yr^{-1}$ reduces ocean acidification by approximately two-thirds by year 2100 (Fig. 3d; Supplementary Information).

Coral reef health is linked to the ocean's aragonite saturation state (Ω_{arg}), which affects the rate at which corals can precipitate this crystalline mineral form of calcium carbonate and build skeletons[13,14]. Modern coral reefs generally occur where open ocean
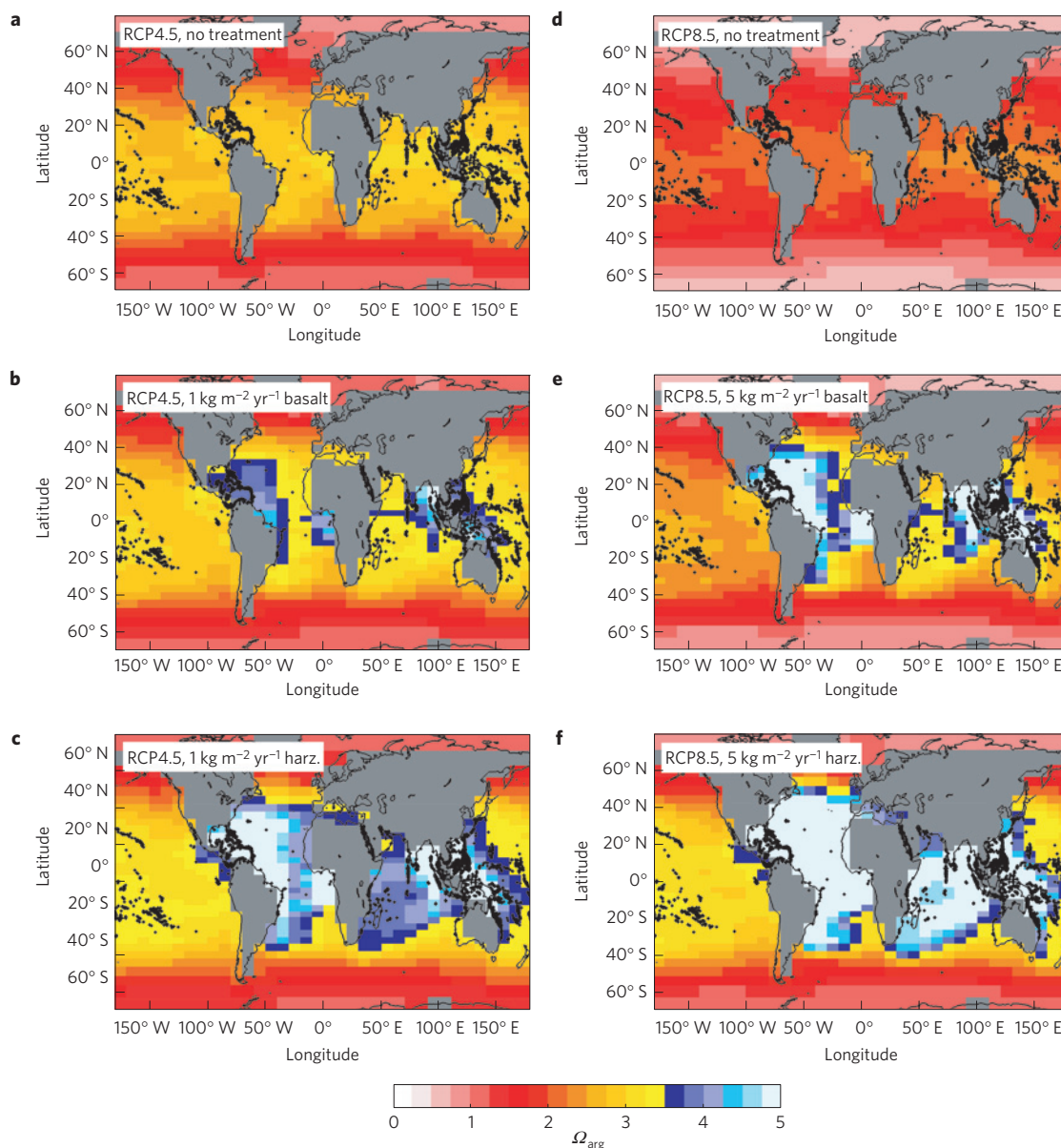
Figure 4 | Enhanced weathering raises the aragonite saturation state of the ocean by 2100. a–c, Simulated global distribution of the aragonite saturation state (Ω_{arg}) of the surface ocean in 2100 for RCP4.5 with no addition of silicate rocks (**a**), and with the addition of $1\,kg\,m^{-2}\,yr^{-1}$ of basalt (**b**) or harzburgite (**c**) distributed over the tropics. **d–f**, Corresponding simulations for RCP8.5 but with applications raised to $5\,kg\,m^{-2}\,yr^{-1}$. In each panel black indicates the distribution of reef-building corals (www.reefbase.org). All simulations are for a mixing depth of 30 cm.

waters have a value of Ω_{arg} above a postulated[14] critical threshold of ∼3.5. But under RCP4.5, and especially RCP8.5, Ω_{arg} at reef sites drops to <3.5 by 2100 (Fig. 4), potentially threatening them with extinction[14]. In simulations for RCP4.5 and RCP8.5, enhanced weathering with $1\,kg\,m^{-2}\,yr^{-1}$ of silicates (basalt or harzburgite) and reduced atmospheric CO_2, generates conditions of $\Omega_{arg} > 3.5$ across main regions of coral reef occurrence (Fig. 4b,c). Hence, although this low dosage is rather ineffective at reducing global CO_2 (Fig. 2), it has specific regional advantages in terms of helping protect coral reefs. Applications of either rock at high rates ($5\,kg\,m^{-2}\,yr^{-1}$) markedly increase Ω_{arg} above 3.5 in both RCP4.5 and RCP8.5 scenarios at low latitudes (Fig. 4e,f). Enhanced weathering on land could therefore be more effective at alleviating stressors on coral reef health, including ocean acidification, than enhanced open ocean dissolution of olivine[26,27].

Our spatial and temporal analyses incorporate detailed plant–soil–climate interactions regulating soil mineral weathering rates.

Driven by detailed geographical variations in projections of twenty-first-century climate change and vegetation activity, they indicate the maximum potential of enhanced weathering for climate change mitigation, including amelioration of ocean acidification. However, our scenarios represent a suite of idealized cases in which application of pulverized silicate rocks over forests is assumed to be achievable over large regions. Consequently, they help define the maximum potential CDR capacity of the approach. Not only will practical barriers to mineral transport and distribution on biodiverse tropical forests limit large-scale deployment, but roll-out on such a large scale may be undesirable from both conservation and ecosystem services viewpoints. Deployment might be achievable in areas undergoing reforestation/afforestation or on agricultural lands where existing infrastructure could be utilized for rock grain distribution and management. However, well-documented field studies on graded spatial scales are needed before any significant implementation.

Large-scale geoengineering is ethically fraught[15] and poses dangers of both foreseeable and unforeseen consequences. Enhanced weathering employs naturally occurring minerals and reactions, and therefore falls in the category of 'soft geoengineering' along with reforestation and agricultural techniques increasing soil carbon storage[28]. Nevertheless, it still requires comprehensive environmental impact assessments and dust mitigation strategies at production and deployment sites. Furthermore, the production and distribution of pulverized rock carries health risks to anyone coming in contact with it because the particle sizes involved are respirable (Supplementary Information). Harzburgite, for example, includes asbestos-related minerals that carry health risks to local populations near application sites. However, carefully implemented, enhanced weathering may have added benefits, including fertilizing ocean and terrestrial CO_2 capture by marine diatoms[3,26,29] and tropical forests, respectively. Such effects, which are not considered here, could help offset energy costs[3,5] associated with extensive rock mining, grinding and transportation operations that might lower its sequestration capacity by ~8–33%.

Estimated implementation costs (combined capital and operational) for achieving an initial 50 ppm drawdown of atmospheric CO_2 are $60–600 trillion for mining, grinding and transportation, assuming no technological innovation, with similar associated additional costs for distribution (Supplementary Information). On this basis, costs of enhanced weathering as a 'negative emissions' option exceed an estimate of $50–200 trillion[17] for air capture of 50 ppm CO_2, but with the latter being less effective in reducing ocean acidification in important coral reef regions. These issues support calls for the alternative of a rising international carbon fee[17]. We proffer enhanced weathering not as a panacea for erasing impacts of fossil fuel burning, but as a sobering indication of actions that may be required if fossil fuel emissions are not phased down rapidly.

Methods

Methods and any associated references are available in the online version of the paper.

References

1. Seifritz, W. CO_2 disposal by means of silicates. *Nature* **345,** 486 (1990).
2. Schuiling, R. D. & Krijgsman, P. Enhanced weathering: An effective and cheap tool to sequester CO_2. *Climatic Change* **74,** 349–354 (2006).
3. Köhler, P., Hartmann, J. & Wolf-Gladrow, D. A. Geoengineering potential of artificially enhanced silicate weathering of olivine. *Proc. Natl Acad. Sci. USA* **107,** 20228–20233 (2010).
4. Hartmann, J. *et al.* Enhanced chemical weathering as a geoengineering strategy to reduce atmospheric carbon dioxide, supply nutrients, and mitigate ocean acidification. *Rev. Geophys.* **51,** 113–149 (2013).
5. Moosdorf, N., Renforth, P. & Hartmann, J. Carbon dioxide efficiency of terrestrial enhanced weathering. *Environ. Sci. Technol.* **48,** 4809–4816 (2014).
6. Taylor, L. L., Banwart, S. A., Leake, J. R. & Beerling, D. J. Modeling the evolutionary rise of ectomycorrhiza on sub-surface weathering environments and the geochemical carbon cycle. *Am. J. Sci.* **311,** 369–403 (2011).
7. Taylor, L. L., Banwart, S. A., Valdes, P. J., Leake, J. R. & Beerling, D. J. Evaluating the effects of terrestrial ecosystems, climate and carbon dioxide on weathering over geological time: A global-scale process-based approach. *Phil. Trans. R. Soc. B* **367,** 565–582 (2012).
8. Cao, L. *et al.* The role of ocean transport in the uptake of anthropogenic CO_2. *Biogeosciences* **6,** 375–390 (2009).
9. Hempel, S., Frieler, K., Warszawski, L., Schewe, J. & Piontek, F. A trend-preserving bias correction—the ISI-MIP approach. *Earth Syst. Dynam.* **4,** 219–236 (2013).
10. Taylor, K. E., Stouffer, R. J. & Meehl, G. A. An overview of CMIP5 and the experiment design. *Bull. Am. Meteorol. Soc.* **93,** 485–498 (2011).
11. Caldeira, K. & Wickett, M. E. Anthropogenic carbon and ocean pH. *Nature* **425,** 365 (2003).
12. Ciais, P. *et al.* in *Climate change 2013: The Physical Science Basis* (eds Stocker, T. F. *et al.*) Ch. 6, 465–570 (Cambridge Univ. Press, 2013).
13. Turley, C. *et al.* The societal challenge of ocean acidification. *Mar. Pollut. Bull.* **60,** 787–792 (2010).
14. Ricke, K. L., Orr, J. C., Schneider, K. & Caldeira, K. Risks to coral reefs from ocean carbonate chemistry changes in recent earth system model projections. *Environ. Res. Lett.* **8,** 034003 (2013).
15. Caldeira, K., Bala, G. & Cao, L. The science of geoengineering. *Annu. Rev. Earth Planet. Sci.* **41,** 231–256 (2013).
16. *United Nations Framework Convention on Climate Change* (1992); http://www.unfccc.int
17. Hansen, J. *et al.* Assessing "dangerous climate change": Required reduction of carbon emissions to protect young people, future generations and nature. *PLoS ONE* **8,** e81648 (2013).
18. *Climate Intervention: Carbon Dioxide Removal and Reliable Sequestration* (Committee on Geoengineering Climate: Technical Evaluation and Discussion of Impacts; Board on Atmospheric Sciences and Climate; Ocean Studies Board; Division on Earth and Life Studies; National Research Council, National Academy of Sciences, 2015).
19. Hartmann, J., Jansen, N., Dürr, H. H., Kempe, S. & Köhler, P. Global CO_2-consumption by chemical weathering: What is the contribution of highly active weathering regions? *Glob. Planet. Change* **69,** 185–194 (2009).
20. Wignall, P. B. Large igneous provinces and mass extinctions. *Earth Sci. Rev.* **53,** 1–33 (2001).
21. Hilf, H. H. Die Düngung mit Basaltabfällen. *Forstarchiv* **14,** 93–101 (1938).
22. de Villiers, O. D. Soil rejuvenation with crushed basalt in Mauritius Part I: Consistent results of world-wide interests. *Int. Sugar J.* **63,** 363–364 (1961).
23. Anda, M., Shamshuddin, J. & Fauziah, C. I. Increasing negative charge and nutrient contents of a highly weathered soil using basalt and rice husk to promote cocoa growth under field conditions. *Soil Tillage Res.* **132,** 1–11 (2013).
24. Gillman, G. P., Burkett, D. C. & Coventry, R. J. Amending highly weathered soils with finely ground basalt rock. *Appl. Geochem.* **17,** 987–1001 (2002).
25. Gasser, T., Guivarch, C., Tachiiri, K., Jones, C. D. & Ciais, P. Negative emissions physically needed to keep global warming below 2 °C. *Nature Commun.* **6,** 7958 (2015).
26. Köhler, P., Abrams, J. F., Völker, C., Hauck, J. & Wolf-Gladrow, D. A. Geoengineering impact of open ocean dissolution of olivine on atmospheric CO_2, surface ocean pH and marine biology. *Environ. Res. Lett.* **8,** 014009 (2013).
27. Hangx, S. J. T. & Spiers, C. J. Coastal spreading of olivine to control atmospheric CO_2 concentrations: A critical analysis of viability. *Int. J. Greenhouse Gas Control* **3,** 757–767 (2009).
28. *Geoengineering the Climate: Science, Governance and Uncertainty* Report No. RS1636 (The Royal Society, 2009).
29. Bernard, C. Y., Dürr, H. H., Heinze, C., Segschneider, J. & Maier-Reimer, E. Contribution of riverine nutrients to the silicon biogeochemistry of the global ocean—a model study. *Biogeosciences* **8,** 551–564 (2011).

Author contributions

D.J.B. conceived the study with input from all co-authors. L.L.T. undertook weathering model development and simulations, J.Q. and R.M.S.T. undertook data analyses, P.A.K. and A.R. provided model set-up support and advice, M.R.L. analysed the CMIP5 climates. D.J.B. led the writing with contributions from all co-authors, especially J.H., A.R., J.Q. and L.L.T.

Competing financial interests

The authors declare no competing financial interests.

Methods

Terrestrial rock weathering modelling. Terrestrial vegetation delivers the carbon-energy flux in the form of photosynthate to roots and associated mycorrhizal fungal networks which fuels biotic rates of mineral dissolution[30]. In our rock weathering model, the subsurface organic carbon flux is stoichiometrically coupled to the rate of primary production and the uptake of inorganic nutrient ions by roots and mycorrhizal fungi which regulate the ionic composition and charge balance of the microscopic region of soil pore fluids at the organism–mineral interface (the mycorrhizosphere)[6,7]. This balance controls local pore fluid pH and organic ligand concentrations at the reacting mineral surfaces that control the rates of mineral dissolution through well-described reaction mechanisms[31]. We therefore couple an extended version of a previously published rock weathering model[6,7] with the Sheffield Dynamic Global Vegetation Model (SDGVM; ref. 32). Our simulations employed fixed land use patterns[33]. The SDGVM simulates terrestrial carbon, nitrogen and water cycling by vegetation and soils, including land surface net primary productivity (NPP), hydrology, autotrophic and heterotrophic soil respiration, and dissolved organic carbon pools[32]. SDGVM is comparable in its sensitivity of response to CO_2 and climate to other DGVMs (refs 34,35).

In the extended weathering model, rainwater with an initial pH determined by the partial pressure and solubility of atmospheric $CO_{2(g)}$ and ion charge balance percolates through the soil at a rate determined by the SDGVM runoff. Soil solution chemistry is calculated both within and outside the mycorrhizosphere within the soil profile, which is divided into ten layers specified at increasing depths, with runoff composition from each layer mixed and advected into the next layer. Mixing of bulk soil and mycorrhizosphere water is conceptualized as, but not explicitly parameterized as, hydrodynamic dispersion and diffusive exchange of bulk soil fluid solutes with the decreasing mycorrhizosphere volume with depth[6], and pore fluid transport to plant roots for transpiration. The model recalculates the soil solution chemistry of each layer, with the dissolution reaction progress of primary silicate minerals ceasing on reaching the theoretical saturation state of the fluid with respect to the dissolving mineral. Thermodynamic equilibria constrain both the forward reaction for mineral dissolution (see equation (1) below) and the concurrent precipitation of secondary phases, including kaolinite, gibbsite and amorphous silica, which act as sinks for dissolved Al and Si released by weathering. On carbonate-bearing lithologies, pore fluids are equilibrated with any calcite, dolomite or gypsum that might be present before weathering of any silicate minerals present takes place. This treatment assumes sufficient carbonates to maintain solubility equilibrium during the simulation time horizon and is not suitable for trace amounts of carbonate minerals, which would become completely depleted in non-carbonate lithologies. Soil solution chemistry, therefore, depends on solubility equilibrium with existing carbonate or sulphate minerals, precipitation of secondary phases, including kaolinite and amorphous silica, and weathering of primary silicate minerals.

Underlying the weathering model is a rasterized version of the Hartmann and Moosdorf[36] lithological map, for which we prepared a lithological database giving the proportions of the parent minerals in each rock type. Each rock type has its own mineral assemblage (see below), and each mineral m weathers according to the general rate law[37] with mineral-specific parameter values for SA, k, n and E:

$$\text{Rate}_m = \text{SA}_m \sum_i \left[k_{i,m}^{298.15} \exp\left[\frac{-E_{i,m}}{R} \left(\frac{1}{T} - \frac{1}{298.15} \right) \right] a_i^{n_{i,m}} \left(1 - \left[\frac{Q_m}{\text{Ksp}_m} \right] \right) \right] \quad (1)$$

where Rate_m is given in mol m^{-2} mineral s^{-1}, SA_m is mineral surface area (m^2), i is the individual weathering agent, such as $[H^+]$, $k_{i,m}$ is the rate constant, $E_{i,m}$ is the apparent activation energy (kJ mol^{-1}), R is the gas constant (kJ mol^{-1} K^{-1}), T is temperature (K), a_i is the molar activity of weathering agent i (mol l^{-1}) and $n_{i,m}$ is the reaction order. $Q_m = \Pi_j a_j^{s_j}$ is the ion activity product of the soil solution, where a_j is the activity of solute j raised to the power of its stoichiometry s_j on the product side of the chemical equation describing the dissolution of mineral m (Supplementary Tables 2 and 3). Ksp_m is the solubility constant for mineral m (Supplementary Table 2). Activities are approximated by concentrations.

The model accounts for changes in mineral surface area due to relief (standard deviation of orography), as described previously[7], and includes an empirical surface area correction for each rock type which accounts for age effects[38], internal porosity, grain size errors and deviation of particle shape from perfect spheres. Soil water residence times and riverine fluxes depend on runoff calculated by SDGVM. The model calculates monthly fluxes of CO_2 consumption, alkalinity (Ca^{2+}, Mg^{2+}, K^+ and Na^+) and dissolved inorganic carbon, and is verified against water chemistry and discharge data from a global suite of river catchments.

Validation. Simulated terrestrial fluxes of CO_2 consumed by rock weathering in 42 watersheds worldwide[39] using the Climate Research Unit 3 (CRU 3) climate[40] at $1° \times 1°$ resolution are validated against fluxes derived from catchment-scale estimates based on stream-water chemistry (Supplementary Information). We generated fluxes for basins in the World Resources Institute's shapefile[41] and compared these to the 45 basins (Table 3 in ref. 39) where the basin names could be matched. Given the test aims to compare model and observed weathering rates,

three catchments were rejected on the basis of markedly different basin areas or runoff (defined as two standard deviations of the mean residual). Therefore, 42 basins were retained for validation, except in the case of carbonate CO_2 consumption, where a further five basins were excluded owing to lack of carbonates in the modelled lithologies.

The response of modelled weathering rates in Iceland to temperature change accords with observed chemical weathering flux responses to climate warming over the past four decades in un-glaciated Icelandic catchments[42]. Regional responses also support the CO_2 and climate change sensitivity of our approach. Adopting a more complex soil weathering module coupled to a DGVM (ref. 43), another group predicted a similar increase in CO_2 consumption in the Mackenzie River Arctic watershed from 355 ppm CO_2 with modern climate to 560 ppm CO_2 with an associated warmer climate, based on results from the RCP4.5 simulations (Supplementary Information). Estimated pH values of river runoff calculated from alkalinity fluxes and equilibrated to ambient CO_2 are comparable to measurements reported for a range of tropical river catchments (Supplementary Information).

Geoengineering simulations. For the atmospheric CO_2 concentration trajectories defined by the two RCPs considered here (RCP4.5 and RCP8.5), the five General Circulation Models (GCMs) produce monthly temperature, relative humidity and precipitation to drive SDGVM. Monthly climate datapoints closest to the desired coordinates are bilinearly interpolated in space before daily values for the month are estimated using climate statistics. These estimated daily climates force SDGVM. Distributed silicate rock grains are treated as perfect monomineralogical spheres with a nominal starting diameter of 10 μm. Initial total surface areas for the added silicates are calculated for each mineral using the total mass applied, specified diameter, weight fraction for the mineral, mineral specific gravity and the equations for the volume and surface area of a sphere. As weathering progresses, mass is removed and the fractional change in total surface area is estimated using the fractional change in mass raised to the power 2/3. This treatment assumes that each particle is a shrinking sphere. The total mass and surface area for each mineral are increased according to dose rate. No attempt is made to model a particle size distribution for either the starting silicate rock grain size or the individual mineral residues following weathering. Pulverized silicates are mixed with a specified depth of soil, without modelling bioturbation processes or the transport behaviour of suspended materials in infiltrating water. Soil water residence times and riverine fluxes depend on runoff modelled by SDGVM. Mean reactive surface areas of autochthonous primary soil minerals are corrected for erosion and relief[7]. The model assumes no change in porosity or water movement with depth, and there is no preferential transport of different particle sizes.

Mineralogy of pulverized silicates. The mineralogy of each simulated pulverized silicate rock is listed in Supplementary Table 4. The model basalt silicate mineralogy is based on the normative composition for a normal alkali tholeiitic basalt[44], neglecting some minor phases such as magnetite. Our dunite composition follows ref. 45. We use the mineralogy of the Troodos harzburgite, with lizardite rather than chrysotile (asbestos), as this is the dominant serpentine near Troodos[46] and as it is sensible to avoid rocks with a large proportion of asbestos for health reasons. Our results are therefore conservative with respect to the proportion of unserpentinized olivine and the relative amounts of lizardite and chrysotile present.

GENIE Earth system global CO_2 and ocean biogeochemistry modelling. The climate and ocean circulation of the GENIE Earth system model has been calibrated by two-dimensional reanalysis fields of surface air temperature and humidity and three-dimensional observational fields of ocean distributions of temperature and salinity[47]. The carbon cycle is calibrated against observed ocean phosphate and alkalinity distributions[47,48]. The resulting marine carbon cycle has been extensively used and evaluated, including against observations of natural (for example, $\Delta^{14}C$) and perturbed anthropogenic carbon cycling. GENIE is also compatible with observational uncertainty[8] and other (generally higher resolution) carbon cycle model responses to CO_2 perturbation[49–51]. The version used here is as summarized by ref. 8, which includes a 76 m deep surface ocean and the cycling of Fe described by Annan and Hargreaves[52] (except with biological uptake following ref. 53), but lacks a mixed layer scheme. Our results therefore represent a pessimistic case for weathering and, in the real world, one might have a slightly shallower surface layer with even higher saturation. The addition of Fe co-limitation of marine biological export results in a less than 1% change in the projected year 1994 anthropogenic CO_2 inventory compared to the PO_4-only model[8].

We simulated the effects of CO_2 consumption by enhanced weathering on atmospheric CO_2 drawdown and ocean biogeochemistry in two steps. First, we diagnosed the annual CO_2 emissions compatible with a particular RCP CO_2 concentration projection over the twenty-first century by prescribing that CO_2 curve and backing-out emissions. Cross-checking these diagnoses by performing forward simulations with annual CO_2 emissions in the absence of enhanced weathering reproduced the RCP4.5 and RCP8.5 CO_2 curves to within 1 ppm. Then,

for each application scenario, we subtracted the annual CO_2 consumption due to enhanced weathering from the diagnosed RCP emissions and forced GENIE with the remainder.

The ocean biogeochemistry simulations incorporate reduced atmospheric CO_2 and increases in the alkalinity and dissolved inorganic carbon fluxes. In each case, those for 2005–2015 and 2089–2099 are transferred to a 36×36 global grid, migrating land fluxes on the weathering model continents to the ocean following standard directional paths. GENIE linearly interpolated these flux forcings for intermediate years. All GENIE runs were based on the same starting state, comprising a 10,000-year pre-industrial spin-up followed by a transient experiment forced by historical changes in atmospheric CO_2 concentration until year 2006, as described in refs 8 and 48.

References

30. Quirk, J., Andrews, M. Y., Leake, J. R., Banwart, S. A. & Beerling, D. J. Ectomycorrhizal fungi and past high CO_2 atmospheres enhance mineral weathering through increased below-ground carbon-energy fluxes. *Biol. Lett.* **10,** 1006–1011 (2014).
31. Brantley, S. L. in *Kinetics of Water-Rock Interaction* (eds Brantley, S. L., Kubicki, J. D. & Art White, F.) Ch. 5, 151–210 (Springer, 2008).
32. Woodward, F. I. & Lomas, M. R. Vegetation dynamics—simulating responses to climatic change. *Biol. Rev.* **79,** 643–670 (2004).
33. Bartholomé, E. & Belward, A. S. GLC2000: A new approach to global land cover mapping from Earth observation data. *Int. J. Remote Sens.* **26,** 1959–1977 (2005).
34. Friend, A. D. *et al.* Carbon residence time dominates uncertainty in terrestrial vegetation responses to future climate and atmospheric CO_2. *Proc. Natl Acad. Sci. USA* **111,** 3280–3285 (2014).
35. Sitch, S. *et al.* Evaluation of the terrestrial carbon cycle, future plant geography and climate-carbon cycle feedbacks using five Dynamic Global Vegetation Models (DGVMs). *Glob. Change Biol.* **14,** 2015–2039 (2008).
36. Hartmann, J. & Moosdorf, N. The new global lithological map database GLiM: A representation of rock properties at the Earth surface. *Geochem. Geophys. Geosyst.* **13,** Q12004 (2012).
37. Palandri, J. L. & Kharaka, Y. K. *A Compilation of Rate Parameters of Water-Mineral Interaction Kinetics for Application to Geochemical Modeling* Report No. 2004-1068, 1–64 (US Geological Survey, 2004).
38. White, A. F. & Brantley, S. L. The effect of time on the weathering of silicate minerals: Why do weathering rates differ in the laboratory and field? *Chem. Geol.* **202,** 479–506 (2003).
39. Gaillardet, J., Dupré, B., Louvat, P. & Allègre, C. J. Global silicate weathering and CO_2 consumption rates deduced from the chemistry of large rivers. *Chem. Geol.* **159,** 3–30 (1999).
40. Mitchell, T. D. & Jones, P. D. An improved method of constructing a database of monthly climate observations and associated high-resolution grids. *Int. J. Climatol.* **25,** 693–712 (2005).
41. *FAO GEONETWORK* (FAO, 2014).
42. Gislason, S. R. *et al.* Direct evidence of the feedback between climate and weathering. *Earth Planet. Sci. Lett.* **277,** 213–222 (2009).
43. Beaulieu, E., Godderis, Y., Donnadieu, Y., Labat, D. & Roelandt, C. High sensitivity of the continental-weathering carbon dioxide sink to future climate change. *Nature Clim. Change* **2,** 346–349 (2012).
44. Nockolds, S. R. Average chemcal compositions of some igneous rocks. *Geol. Soc. Am. Bull.* **65,** 1007–1032 (1954).
45. Kogel, J. E., Trivedi, N. C., Barker, J. M. & Krukowski, S. T. *Industrial Minerals and Rocks—Commodities, Markets, and Uses* 7th edn (Society for Mining, Metallurgy, and Exploration, 2006).
46. Magaritz, M. & Taylor, H. P. Oxygen and hydrogen isotope studies of serpentinization in Troodos ophiolite complex, Cyprus. *Earth Planet. Sci. Lett.* **23,** 8–14 (1974).
47. Price, A. R., Myerscough, R. J., Voutchkov, I. I., Marsh, R. & Cox, S. J. Multi-objective optimization of GENIE Earth system models. *Phil. Trans. R. Soc. A* **367,** 2623–2633 (2009).
48. Ridgwell, A. *et al.* Marine geochemical data assimilation in an efficient Earth System Model of global biogeochemical cycling. *Biogeosciences* **4,** 87–104 (2007).
49. Archer, D. *et al.* Atmospheric lifetime of fossil fuel carbon dioxide. *Annu. Rev. Earth Planet. Sci.* **37,** 117–134 (2009).
50. Eby, M. *et al.* Historical and idealized climate model experiments: An intercomparison of Earth system models of intermediate complexity. *Clim. Past* **9,** 1111–1140 (2013).
51. Goodwin, P., Williams, R. G., Ridgwell, A. & Follows, M. J. Climate sensitivity to the carbon cycle modulated by past and future changes in ocean chemistry. *Nature Geosci.* **2,** 145–150 (2009).
52. Annan, J. D. & Hargreaves, J. C. Efficient identification of ocean thermodynamics in a physical/biogeochemical ocean model with an iterative Importance Sampling method. *Ocean Model.* **32,** 205–215 (2010).
53. Doney, S. C., Lindsay, K., Fung, I. & John, J. Natural variability in a stable, 1000-yr global coupled climate—carbon cycle simulation. *J. Clim.* **19,** 3033–3054 (2006).